Research article

Effect of the thermal processing on the microstructural, functional and mechanical properties of cast polycrystalline NiMnTi alloys

Francesca Villa [a,b,*], Elena Villa [a], Lara Righi [c], Pietro Ruggieri [d], Nicola Bennato [a], Simone Battiston [e], Francesca Passaretti [a], Riccardo Casati [b]

[a] CNR ICMATE, Lecco Unit, Italy
[b] Politecnico di Milano, Department of Mechanical Engineering, Italy
[c] Università di Parma, Department of Chemistry, Life Sciences and Environmental Sustainability, Italy
[d] Università degli studi di Milano Bicocca, Department of Materials Science, Italy
[e] CNR ICMATE, Padova Unit, Italy

ARTICLE INFO

ABSTRACT

The solid-state refrigeration and heat pumping field is gaining increasing attention as an alternative solution to the conventional vapour-based cooling devices. Among the shape memory alloys (SMAs), besides the reference NiTi system, outstanding elastocaloric performances are exhibited by the NiMnTi alloy. In this work, we produced two cast NiMnTi alloys which were characterized in terms of microstructural, structural, functional, and mechanical properties. Moreover, we assessed the effect of the heat treatments on the microstructure and on the physical properties of the produced alloys by calorimetric, structural and high-temperature microscope analyses. Furthermore, the heat treatments promoted partial mechanical cycling stability and a superelastic behavior without significant residual strains. Finally, the elastocaloric performance of the alloy was evaluated by direct adiabatic ΔT measurements upon elastocaloric cycles in four different loading conditions. The alloys exhibited promising elastocaloric performance for possible solid-state cooling applications. In particular, the best adiabatic ΔT value achieved in this work was 8.7 °C with a strain rate of 400 %/min and up to a strain of 5 % for the NiMnTi heat treated at 900°C.

1. Introduction

The solid-state refrigeration and heat pumping technologies based on the use of caloric materials are gaining increasing attention as a valid and sustainable alternative to the traditional vapor compression-based techniques [1]. In particular, the elastocaloric cooling is considered one of the most promising options due to some advantages that include the compactness and simplicity of operation, the reduced environmental impact and the high efficiency [2–5]. Indeed, elastocaloric devices can reach levels of efficiencies similar to those of the traditional systems [6] and do not involve the use of harmful fluids that can be dispersed in the environment [7]. Among caloric materials, the superelastic shape memory alloys (SMAs) are the most promising candidates [8] for the development of elastocaloric systems. Indeed, they are characterized by a first-order reversible solid-state transformation which involves a high latent heat. This transition is called thermoelastic martensitic transformation (TMT) and can be induced by a change in temperature or by

the application of a deformation [9,10]. Therefore, it is possible to adiabatically load such materials to induce the TMT and allow them to heat up. The heat generated in the material can be removed and stored or dissipated depending on the kind of effect to be exploited. Then, since the TMT is reversible upon removal of the load, the inverse transformation takes place, the material cools down and the generated heat is removed [11–13]. The adiabatic conditions during mechanical loading stages are reached by rapidly applying and removing the deformation, with strain rates over 0.05 1/s [12]. Since in this way the adiabatic conditions are approximated, it is possible to define them as quasi-adiabatic. The caloric effects can be described by two parameters, i.e. the total change of temperature in adiabatic conditions (ΔT_{ad}) and the total change of entropy in isothermal conditions (ΔS_{iso}) and a co-efficient of performance (COP) can be evaluated [8,11,12,14].

Among the SMAs, one of the emerging alloys for elastocaloric purposes is the Heusler *all-d-metal* NiMnTi, which is composed only of elements from the *3d* group [15,16]. This alloy is not characterized by the

typical brittleness of the intermetallics generated by the strong covalent interaction between the constitutive elements caused by the *p-d* orbital hybridization. Indeed, in NiMnTi, the *d-d* hybridization takes place and the valence electrons are uniformly distributed and generate a metallic bonding [17,18]. These features give rise to improved mechanical properties with respect to other Heusler alloys, including relevant superelasticity up to 7 % and high elongation at break up to 13 % [17,19, 20]. Moreover, the large unit cell volume change ($\Delta V/V_0$) between the austenitic and martensitic phases that characterizes this alloy induces a high entropy change and therefore good elastocaloric properties [21]. However, the high volume change during the transformation could inhibit the transformation reversibility due to the possible formation of static misfit dislocations [22,23].

Considering arc melted NiMnTi alloys, literature offers limited studies concerning their physical and elastocaloric properties. In reference [24], cast samples were subjected to deformations of up to 3.9 %, achieving an irreversible adiabatic temperature change (ΔT) of 10.7°C. Another study [25] achieved higher adiabatic ΔT values, reaching up to 17°C under high applied strain (7 %). Furthermore, the addition of boron (B) to the polycrystalline cast alloy resulted in temperatures of up to 31.5°C, as reported in [21]. This latter case is an example of the possibility to enhance the elastocaloric properties of the alloys. In fact, the effect of the B micro-alloying is a significant grain refinement and a consequent increase of the NiMnTi mechanical properties, as observed for other alloys [26]. Another strategy to improve the caloric properties consists in the reduction of the stress hysteresis through the formation of non-transforming phases resulting in a nanocomposite microstructure [27]. Finally, it is possible to introduce microstructure texturing, e.g. through directional solidification [28], to achieve colossal caloric effects. In particular, it is possible to find some experimental studies on NiMnTi samples produced by Bridgam method which exhibit adiabatic ΔT ranging from 20.4 °C [17] to 37.3 °C [25].

The effect of the amount of Ti on the transformation temperatures was studied by Cong et al. [21] and it was found that by increasing the amount of Ti, in replacement of Mn, the transformation temperatures decrease. In addition, in [17] the formation of $(Ni,Mn)_3Ti$ precipitates in heat treated samples is experimentally observed. It is expected that, as for NiTi alloys [29], the precipitates could affect the cycling stability of the alloy, acting as obstacles to the mobility of dislocations and therefore improving the functional stability upon thermo-mechanical cycling [29, 30]. Moreover, the precipitates could act as energy barriers to the Martensite formation, being responsible for a tilted plateau in the stress-strain curves [29,31]. No comparisons between polycrystalline samples with thermo-mechanical optimization of the microstructure are actually present in literature. Furthermore, it is important to highlight that, in view of possible applicative developments, a complete investigation of polycrystalline alloy produced by a low cost, large scale and reproducible method is a fundamental step. Moreover, this approach allows the complete study and control of key parameters to develop the best functional properties.

In the current work, two different polycrystalline NiMnTi alloys were produced by arc melting and heat treated to achieve different microstructural configurations. Thermal, calorimetric, and structural analyses were performed to evaluate the effect of the thermal treatments on the TMT and the microstructure of the alloy. For the alloys that proved to be more suitable for room temperature elastocaloric applications, a mechanical characterization including both isothermal and quasi adiabatic measurements is presented to give a perspective for possible solid-state cooling or heat pumping purposes. This is a new and promising field of the scientific research about the SMAs. Moreover, it is important to point out that the study of the intrinsic properties of these materials, from the microstructural and functional point of view, is a fundamental step for the development of solid-state cooling devices. Therefore, the current study aims at boosting the fundamental knowledge about the NiMnTi alloy produced by means of a cost-effective and traditional process. In this way, it is possible to lay the foundations for further development of advanced production and processing routes for this material.

2. Materials and methods

Two series of NiMnTi ingots with two different compositions (namely, $Ni_{50}Mn_{35}Ti_{15}$ and $Ni_{50}Mn_{32}Ti_{18}$ in atomic %) were produced by means of a non-consumable electrode vacuum arc furnace from metallic elements with purity higher than 99 %. The ingots were produced under Ar atmosphere into a water-cooled copper crucible, and they were re-melted six times to provide homogeneous chemical composition. The as-cast samples have been labelled as "NMT15_AC" and "NMT18_AC".

The homogeneity of the chemical composition of the as-cast samples was evaluated by means of the INCA Energy 200 dispersive X-Ray spectroscopy (EDS) equipment mounted on a LEO 1430 scanning electron microscope (SEM). The thermal and calorimetric analysis was carried out by means of a differential thermal analyzer (DTA) Q600 TA Instruments in Ar atmosphere with a heating and cooling rate of 25 °C/ min and differential scanning calorimeter (DSC) DSC25 TA instruments with a heating and cooling rate of 10 °C/min. The transformation temperatures were identified at the intersection point between the tangent line to the baseline and to the inflection point of the heat flow peaks, which is the well-known procedure generally established in calorimetric analysis. The *in-operando* morphological characterization was performed at 600 °C using a Sigma Zeiss Field Emission Scanning Electron Microscope (FE-SEM), equipped with a Kammrath & Weiss heating module. The room temperature microstructural observation was carried out through Leitz Aristomet optical microscope and SEM LEO 1430 scanning electron microscope on polished and etched samples. The etching solution was composed by 60 vol% of distilled water, 35 vol% of nitric acid and 5 vol% of hydrofluoric acid. Thermal treatments were carried out on samples put into quartz vials with argon atmosphere. The thermal treatments were followed by water quench and all the treatments conditions are resumed in Table 1.

The X-Ray diffraction (XRD) analysis was carried out on bulk samples by means of an X-Ray Diffractometer Panalytical XPert PRO equipped with a thermal chamber for measurements below and above room temperature, for the study of the martensitic and parent phases. The high-resolution transmission electron microscopy (HR-TEM) imaging was performed with a ThermoFisher Talos F200X TEM. The thin samples for TEM analysis were prepared by means of the METALTHIN twin jet electropolishing system using a solution composed by 90 vol% of methanol and 10 vol% of perchloric acid cooled down at −20 °C. The compressive isothermal mechanical measurements were performed by means of an MTS 2/M universal testing machine equipped with a load cell of 10 kN, in compression configuration. The measurements were performed in strain control mode and strain rate was 1 %/min. The same instrument was used for the elastocaloric measurements, that were carried out with strain rates of 150 and 400 %/min. An ad hoc setup with thermocouples and a high-frequency acquisition system [32,33] was used for the evaluation of the adiabatic ΔT.

3. Results

The chemical composition was measured on as-cast ingots through EDS analysis and the results are reported in Table 2. It was observed that the composition is homogeneous along the entire cross sections of the samples. Moreover, no significant Mn loss was registered after casting.

Differential thermal analysis was performed on as-cast samples to identify the exothermal and endothermal transformations that take place upon heating. The results are shown in Fig. 1(a) and Fig. 1(b). The melting temperature was 1108 °C and 1119 °C for NMT15 and NMT18 respectively. In addition, it is possible to observe one exothermal peak for each alloy that can likely related to the formation of secondary phases such as Ni-Ti-based precipitates [15]. These peaks are spread over a wide temperature range and are not sharply pronounced with

Table 1

Summary of the samples obtained after thermal treatments applied to NMT15_AC and NMT18_AC.

Sample	Alloy (at%)	Temperature (°C)	Time (h)	Atmosphere	Cooling
NMT15_600°C_2h	$Ni_{50}Mn_{35}Ti_{15}$	600	2	Ar	Water quench
NMT15_900°C_48h	$Ni_{50}Mn_{35}Ti_{15}$	900	48	Ar	Water quench
NMT15_1000°C_24h	$Ni_{50}Mn_{35}Ti_{15}$	1000	24	Ar	Water quench
NMT18_600°C_2h	$Ni_{50}Mn_{32}Ti_{18}$	600	2	Ar	Water quench
NMT18_900°C_48h	$Ni_{50}Mn_{32}Ti_{18}$	900	48	Ar	Water quench
NMT18_1000°C_24h	$Ni_{50}Mn_{32}Ti_{18}$	1000	24	Ar	Water quench

Table 2

Mean values of the atomic composition evaluated through EDS analysis on the cross sections of the NiMnTi as-cast ingots. The values in brackets correspond to the standard deviation.

Sample	Ni (atomic %)	Mn (atomic %)	Ti (atomic %)
NMT15_AC	50.1 (0.1)	34.5 (0.2)	15.4 (0.2)
NMT18_AC	49.9 (0.2)	31.6 (0.2)	18.5 (0.3)

respect to the baseline signal. To further investigate the formation of such second phases, the thermal analysis was supported by high-temperature SEM microscopy (Fig. 1(c), (d), 1(e) and 1(f)). Only the micrographs taken at 600 °C after 90 minutes of temperature holding, reported in Fig. 1(e) and (f), show the formation of sub-micrometric precipitates. These particles are more visible and coarser in sample NMT15_AC. Further DTA isothermal measurements were carried out at different temperatures for 2 hours and the heat flow signal versus time is shown in the inset of Fig. 1(a) for sample NMT15_AC. These measurements proved that, after 80–90 minutes, a change in the heat flow, and therefore in the specific heat, is visible at 600 °C and even more at 900 °C, likely corresponding to a significant formation of precipitates. It is worth to consider that the isothermal measurements are interesting to observe the heat capacity change which occurs above 600°C. The time correspondent to this phenomenon is not

significant, because it is due to the complete thermalization time and to the thermal transition in samples with different weights.

For a detailed investigation of the calorimetric properties of the two alloys in the temperature range of the TMT, DSC analysis was performed. Fig. 2 shows the DSC curves of the as-cast and heat treated samples with composition NMT15 and NMT18. The as-cast samples show very broad and spread peak over a wide range of temperatures. Samples treated at 600°C for 2 hours show similar curves. In both cases, the critical transformation temperatures were determined with the tangent method to identify the onset points of the wide peaks. Furthermore, heat treatments at higher temperatures and longer times promoted narrower TMT peaks with easily identified onset points. Moreover, it is possible to observe that the peaks are shifted towards higher temperatures with the increase of the soaking temperature. Table 3 resumes the TMT temperatures and enthalpies of the investigated samples.

The as-cast microstructure of NMT15 and NMT18 alloys is reported in Fig. 3(a), showing dendritic microstructure. Dendrites are also noticeable in the samples treated at 600 °C (Fig. 3(b)), while they dissolve during thermal treatments at higher temperatures (Fig. 3(c) and Fig. 3(d)), revealing that heat treatment at temperature of 900 and 1000°C are able to homogenize the microstructure. Moreover, it is possible to observe that in the samples treated at 900 °C some precipitates are still visible both at the grain boundaries and cores.
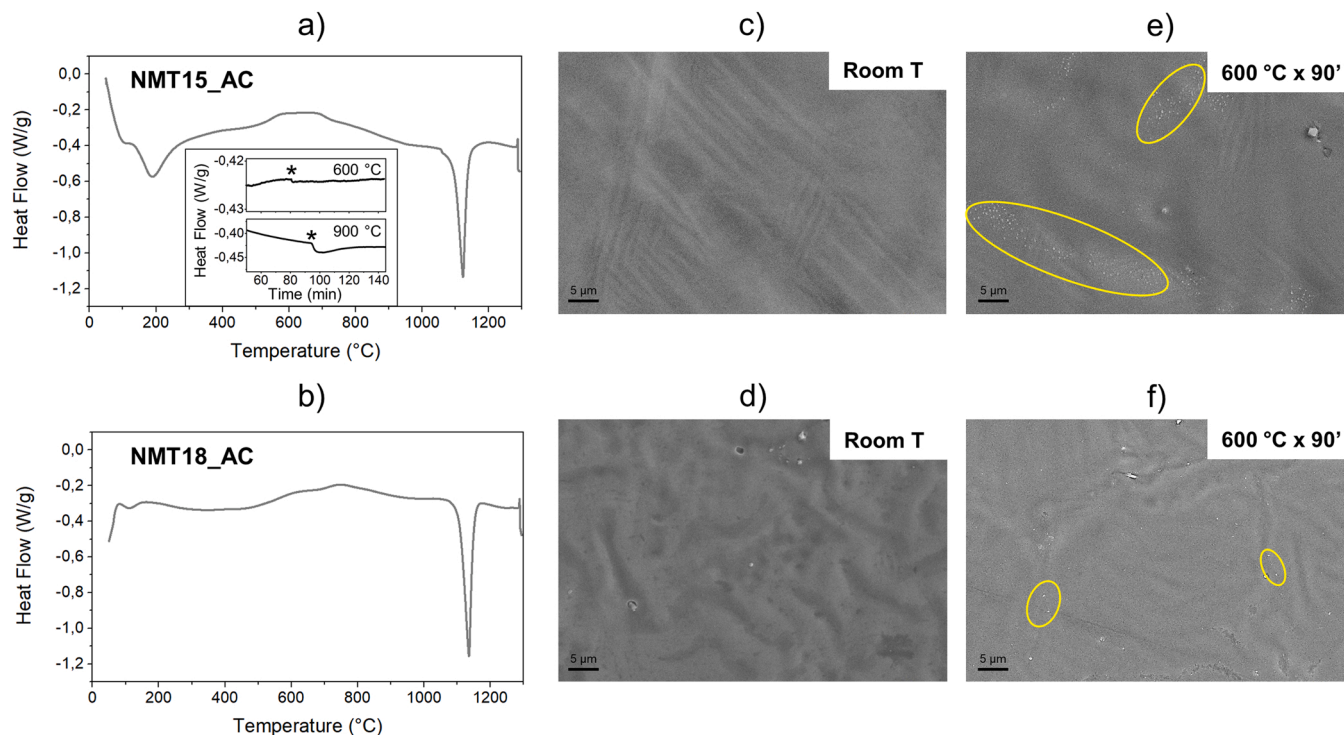

Fig. 1. Differential thermal analysis (DTA) (a, b) and SEM micrographs at room temperature (c, d) and 600 °C (e, f) for samples NMT15_AC and NMT18_AC. Exothermal direction: up. The inset in (a) shows the heat flow signal vs. time during isothermal measurements at 600 and 900 °C. The asterisks indicate the signal changes.
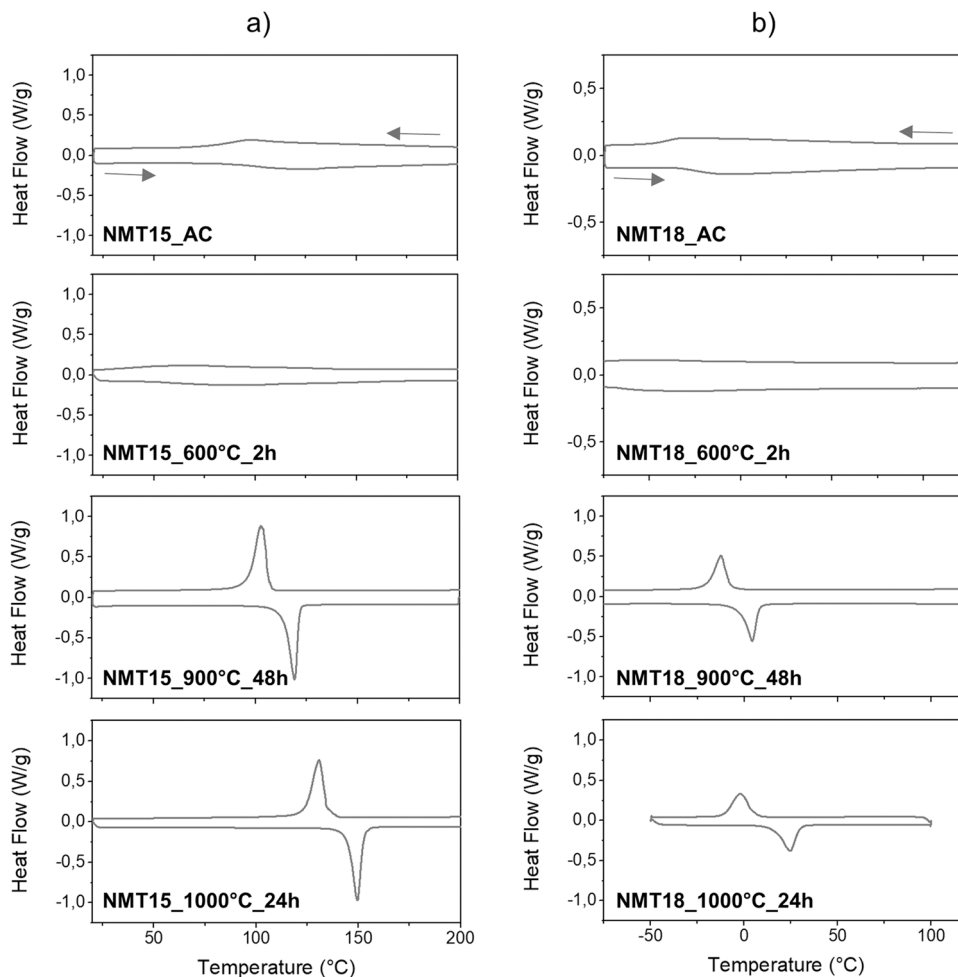
Fig. 2. Differential scanning calorimetry (DSC) for NMT15 alloy (a) and NMT18 alloy (b). Exothermal direction: up.

Table 3
Summary of the martensite start (Ms) and finish (Mf) temperatures, austenite start (As) and finish (Af) temperatures and enthalpies upon cooling and heating obtained from DSC data.

Sample	M_s (°C)	M_f (°C)	A_s (°C)	A_f (°C)	ΔH_{cool} (J/g)	ΔH_{heat} (J/g)
NMT15_AC	200.9	71.6	86.3	204.8	34.7	29.2
NMT15_TT600°C_2h	148.4	25.7	48.3	176.5	29.1	23.8
NMT15_TT900°C_48h	107.3	95.2	113.2	121.5	34.7	30.9
NMT15_TT1000°C_24h	134.6	122.9	143.6	152.7	31.6	30.0
NMT18_AC	88.7	-49.3	-34.5	103.2	23.4	23.2
NMT18_TT600°C_2h	24.2	-88.3	-72.2	45.1	15.1	13.7
NMT18_TT900°C_48h	-7.1	-20.3	-3.3	8.1	21.4	21.2
NMT18_TT1000°C_24h	6.2	-10.9	15.0	29.9	18.4	18.0

Conversely, the samples treated at 1000 °C show no second phases.

The structural investigation of NiMnTi alloys was conducted through XRD analysis at different temperatures, in order to study the evolution of the crystal structure above and below the TMT. As an example, the XRD patterns of the samples NMT18 and NMT15 heat treated at 900 °C are reported in Fig. 4. For sample NMT15_900C_48h, the diffraction pattern at 25 °C reveals the martensitic structure with the multiplet between 40 ° and 45 ° typical of NiMn-based Heusler alloys. Moreover, an intense peak related to Ni_3Ti precipitates is identified at 46.5 °. The same peak is visible also in the pattern registered at 170 °C, namely above the TMT. In this case, the austenitic cubic structure was identified in correspondence of the intense peak indexed as (200) reflection. However, it is possible to notice that some less intense peaks related to the martensitic phase are still present close to the principal austenitic reflection. This means that

residual martensite is present in the sample heated above the TMT at 170 °C. In the case of NMT18 alloy, it was necessary to cool the material down to - 80 °C in order to investigate the martensitic structure and, also for this composition, the multiplet and the Ni_3Ti signal are detected. Both the patterns registered at room temperature and 170 °C show the (200) and (400) austenitic reflections and some minor peaks related to residual martensite, especially at room temperature.

In order to further investigate the martensitic structure of NiMnTi alloy, the as-cast samples were analyzed by XRD below the TMT and the results are reported in Fig. 5. The Lebail fitting [34] on XRD patterns indicated that martensite has an orthorhombic symmetry with 5 M modulation with a **q** modulation vector close to 2/5 periodicity, and it was possible to determine the unit cell constants which are reported in Table 4. These results are in agreement with previous structural studies
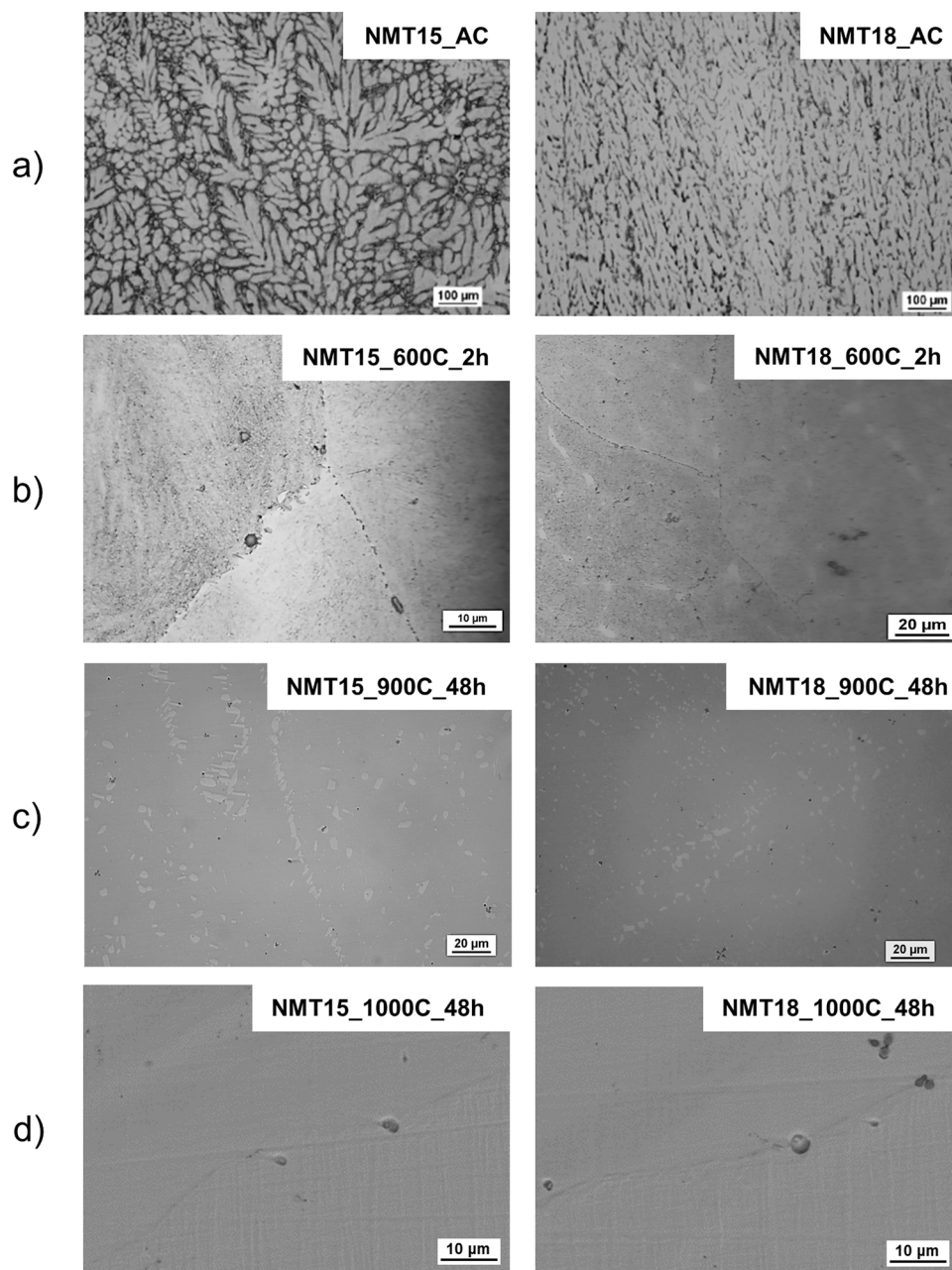
Fig. 3. Room T optical micrographs of the NiMnTi samples: (a) as-cast, (b) thermally treated at 600 °C, (c) thermally treated at 900 °C and (d) thermally treated at 1000 °C.

[35]. Moreover, it was possible to determine the modulation vector just for sample NiMnTi15_AC because it showed a higher crystallite size of the crystalline phase.

The average crystallite size of martensitic phase was obtained by the classical Sherrer approach, and it corresponded to 26(4) and 11(5) nm for NiMnTi15_AC and NiMnTi18_AC, respectively. It is worth to recall that the crystal size assigned by XRD is related to the dimension of the domains coherently diffracting. In a first approximation such information could be related to the extension of the martensitic nano-twins hierarchically distributed. Moreover, in both cases, also the Ni_3Ti phase was observed, meaning that some precipitates are already present in the as-cast alloy.

In addition, HR-TEM analysis at room temperature was performed to further investigate the martensitic microstructure of NiMnTi alloys. For this purpose, the NiMnTi15 alloy was analyzed since it is in the martensitic phase at room temperature. A transmission micrograph of a thin NMT15_AC sample is reported in Fig. 6 and it shows the features typical of martensite composed by several substructures. This architecture confirms the information about the small crystallite sizes obtained from the XRD data of the martensitic phase.

Fig. 7(a) shows the isothermal compressive curves for the sample NMT18_TT900°C_48h. At room temperature this sample shows superelastic behavior with the typical flag-shaped curve. However, a residual strain of 1 % after the first cycle can be observed. This is because microstructural features such as precipitates or grain boundaries may act as barriers to the reverse transformation during unloading, hindering the complete transformation of martensite [29]. After five further cycles, the curve shows no residual deformation and a maximum value of strain of 4.0 % was reached with an applied stress of 450 MPa. The loading stage is not fully stabilized, but stability upon unloading is consistently observed even after a small number of cycles. As a result, the mechanical loop has achieved acceptable stability for further analysis. After such
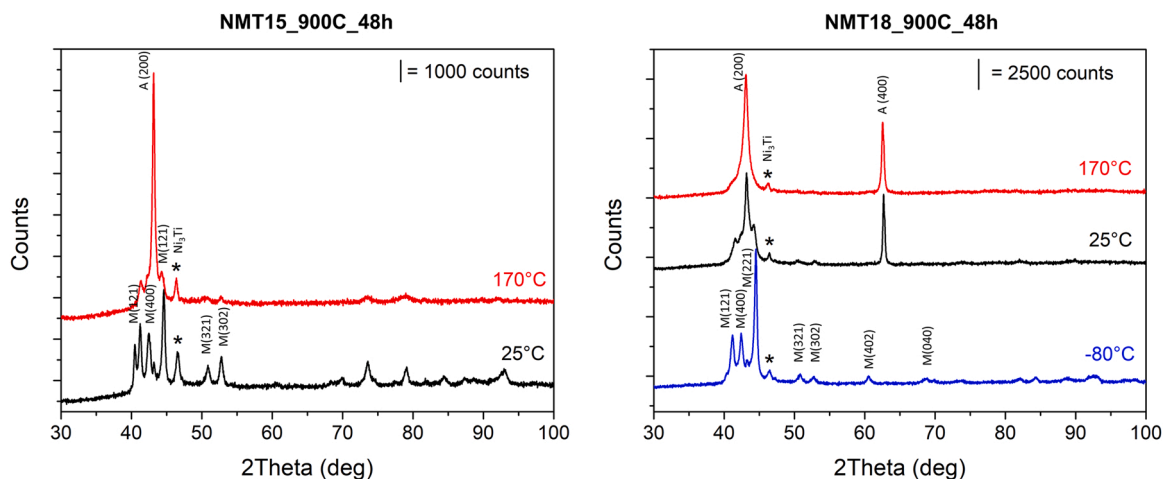
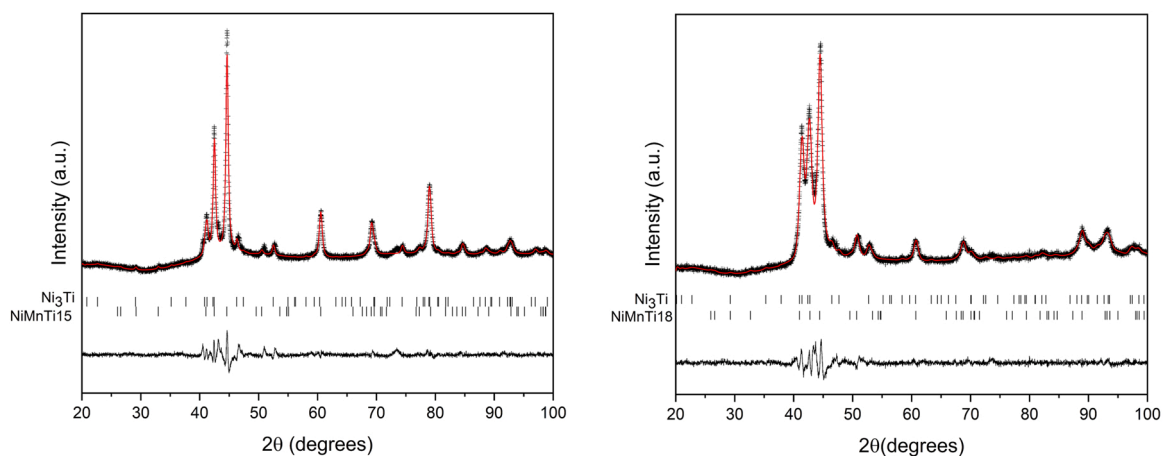**Fig. 4.** XRD analysis at various temperatures of NiMnTi samples thermally treated at 900 °C for 48 hours.

Fig. 5. Lebail fitting on XRD patterns for as-cast NiMnTi samples below the TMT (-80 °C for NiMnTi15 and room T for NiMnTi18).

Table 4
Unit cell constants (in Å) and modulation vector determined for samples NiMnTi15_AC and NiMnTi18_AC. The numbers in brackets represent the uncertainty on the last digit.

sample	a	b	c	q
NiMnTi15_AC	4.3982(1)	5.430(2)	4.2528(3)	0.398(2) x c
NiMnTi18_AC	4.3650(2)	5.482(5)	4.2220(7)	/

first cycles, a series of compression tests in quasi-adiabatic condition were performed on the same sample. A combination of different applied strains and strain rates was selected to investigate the influence of these parameters on the generated adiabatic ΔT. The results are summarized in Fig. 7(b) and, as expected, there was an increase of the ΔT at higher applied strains and at higher strain rates. The maximum positive ΔT value obtained was 8.7 °C and the maximum negative ΔT was 4.5 °C.

4. Discussion

The DTA analysis performed on as-cast samples (Fig. 1(a) and (b)) revealed the presence of exothermal reactions that occurred upon heating, but the weak nature of signals necessitated further investigation by SEM at high temperature (Fig. 1(d) and (e)). It was directly observed that after 1.5 h at 600°C, some particles precipitated at grain boundaries and within the grains. The change in specific heat observed in the isothermal DTA curves at 600 °C and at 900°C confirmed the formation
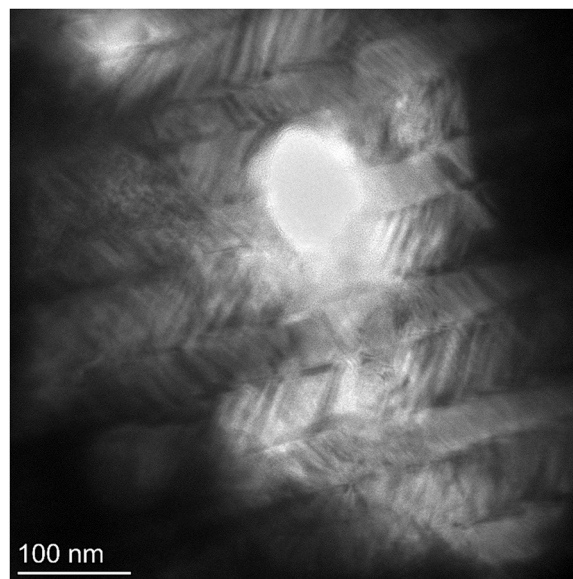

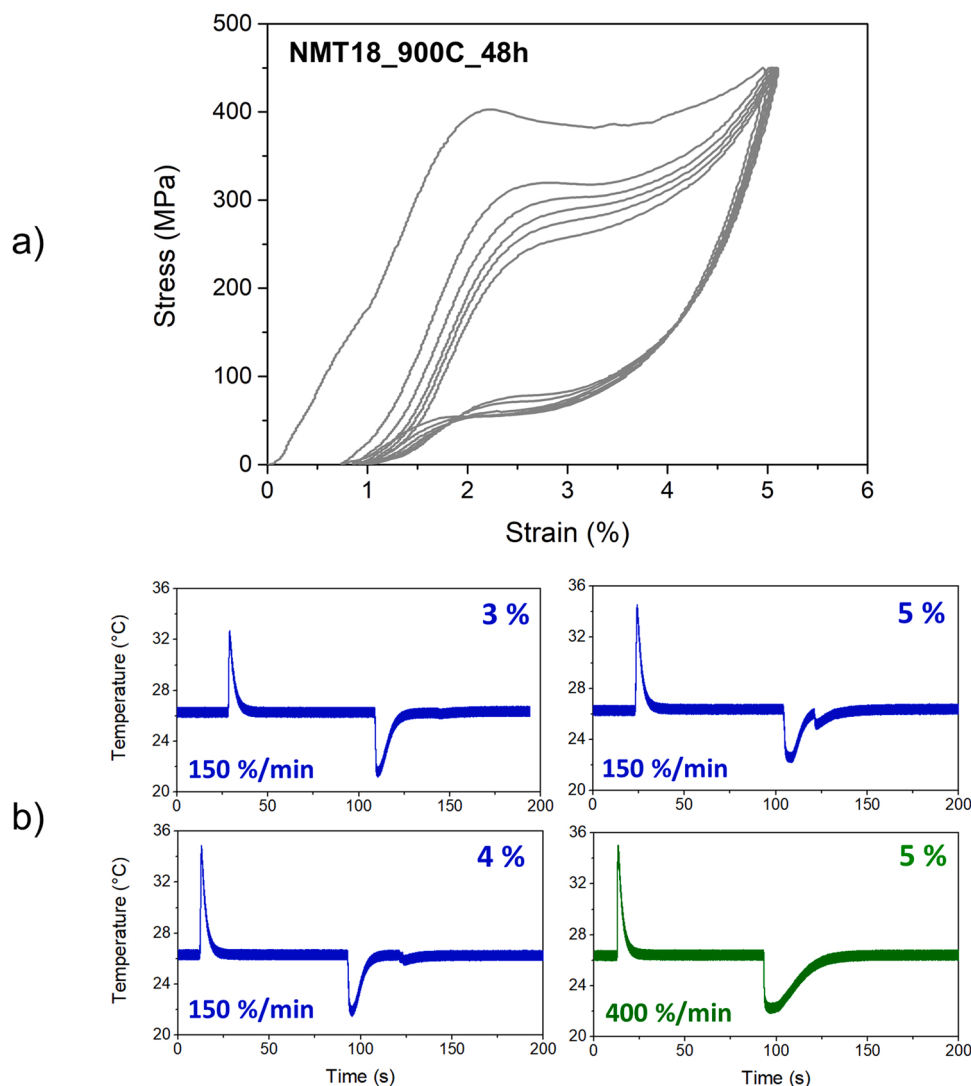**Fig. 6.** TEM micrograph of sample NMT15_AC registered at room temperature.

Fig. 7. Isothermal compression stress-strain curves at room temperature (a) and temperature profiles registered on the sample surface at different strains and strain rates (b) for sample NMT18_TT900°C_48h.

of precipitates in this range of temperatures. Considering these preliminary results, NiMnTi samples with 15 and 18 % of Ti were heat treated at 600, 900 and 1000°C. From the calorimetric point of view (Fig. 2), the thermal treatment at 600 °C for 2 h did not have effect on the TMT because for both alloys the peak related to the transformation remains wide and spread over a wide temperature range. Consistently, looking at the microstructure in Fig. 3, it was possible to identify the presence of the dendritic structures. This means that the short time and low temperature of this heat treatment were not enough to homogenize the cast microstructure. The soaking at 900 °C promoted the formation of precipitates and from the calorimetric data it was possible to observe that the TMT occurred in a narrower range of temperatures. Such treatment was able to homogenize the microstructure and promote the formation of precipitates. The thermal treatment performed at 1000 °C induced the narrowing of the TMT peak in DSC signal, its shift towards higher temperatures and the absence of precipitates.

The XRD analysis at different temperatures (Fig. 5) provides an insight into the evolution of the crystal structure of the thermally treated samples below and above the TMT. In the case of the sample treated at 900 °C, some residual martensite was visible in the high temperature patterns. It could be blocked by the presence of impurities, such as Ti oxides, and precipitates that create discontinuity in the microstructure and compositional gradients that locally hinder the transformation [36].

The precipitates in the samples treated at 900 °C were identified as Ni_3Ti phase, in agreement with [17]. Going into the details of the as-cast martensitic phase, the alloy with higher Ti concentration (18 %) presented grains with slightly lower dimensions. Moreover, the excess in Ti might have played as a barrier to the martensite growth. Moreover, it was possible to directly observe the martensitic structure on thin samples at high magnifications with TEM. The representative micrograph reported in Fig. 6 for NMT15_AC showed the presence of twin substructures in the martensite as seen for other Heusler alloys and NiMnTi [16,37]. This was in accordance with the structural analysis that allowed to evaluate an average crystal size of 26 nm for NiMnTi15_AC.

Considering room temperature solid-state heating and cooling applications, the best performing alloy was that with 18 % of Ti and treated at 900 °C due to several factors. Firstly, its A_f temperature is well below the desired operation temperature (see Table 2) and therefore the austenite phase is stable in that condition. Then, it exhibits a good superelastic behavior at room temperature since it is possible to apply strains up to 4 % with no residual strains upon unloading, as reported in Fig. 7(a). Moreover, the chosen alloy exhibits cycling stability for the formation of stress-induced martensite upon several cycles. The isothermal stabilization cycles were necessary to reduce residual strains, so the subsequent adiabatic compressions were performed on stabilized samples. The theoretical maximum achievable adiabatic ΔT can be

evaluated considering the latent heat involved in the TMT and measured by calorimetry, as reported in equation 1 [38].

$$\Delta T^{th} = \frac{\Delta H}{c_p}$$

The theoretical ΔT of sample NMT18_TT900°C_48h evaluated using a reference c_p for this alloy [17] is equal to 42 °C. The discrepancy between the positive and negative experimentally measured ΔT (Fig. 7(b)) and the theoretical one could be ascribed to the non-perfect adiabatic conditions. Moreover, in the case of the compression tests, the stress-induced martensitic transformation could be affected by the presence of microstructural discontinuities such as precipitates, impurities, and grain boundaries. Therefore, the activation energy of the stress-induced TMT, could be more influenced by the microstructural features of the alloy with respect to the thermally-induced TMT [32,33]. Furthermore, the heat transmission inside massive compression samples towards the surface could decrease the registered ΔT. Finally, the observed deviation between positive and negative adiabatic ΔT could be ascribed to the mechanical and thermal hysteresis typical of these alloys. Indeed, it is possible to assume that, during adiabatic loading, an intrinsic mechanical dissipative heat due to the internal friction is generated in addition to the latent heat of the phase transformation. Assuming all dissipative energy transforms into heat, this hysteresis loss leads to asymmetry in the adiabatic ΔT during rapid loading and unloading. Additionally, temporary residual strains caused by the presence of residual martensite, as described in [39], contribute further to this temperature irreversibility. However, the maximum positive and negative registered ΔT, i.e. 8.7 and - 4.5 °C, are considered as promising values for a polycrystalline alloy produced with conventional method for a perspective of application in the room temperature solid-state heat pumping and cooling fields.

5. Conclusions

In the current work, two NiMnTi alloys, namely $Ni_{50}Mn_{35}Ti_{15}$ and $Ni_{50}Mn_{32}Ti_{18}$ (in atomic %), were successfully produced by arc melting. From the thermal analysis and *in-operando* SEM analysis it was found that precipitation of a Ni-Ti based phase occurs between 600 and 900 °C. The calorimetric analysis and the microscopic observation revealed that the microstructural condition and the TMT was tuned by heat treatments at 600, 900 and 1000 °C. In particular, after the low temperature heat treatment, dendritic structures were still present and some precipitates were formed. Secondly, the high temperature heat treatments promoted the alloy homogenization with a narrowing of the TMT temperatures. In the case of the heat treatment at 900 °C, Ni-Ti based precipitates were formed at grain boundaries and within the grains. The alloy with 18 % of Ti and heat treated at 900 °C presented the best compromise between the microstructure homogenization and transformation temperatures for room temperature elastocaloric applications. After the stabilization cycles, the adiabatic ΔT was directly measured on the sample surface using different combinations of applied strains and strain rates. The maximum positive ΔT of 8.7 °C and the negative one of 4.5 °C were the promising measured values for this polycrystalline cast NiMnTi alloy. In conclusion, the current work contributes to the improvement of the fundamental knowledge about the NiMnTi cast alloy which could be a precursor material for subsequent possible processing routes for application devices.

CRediT authorship contribution statement

Simone Battiston: Investigation. **Francesca Passaretti:** Supervision. **Riccardo Casati:** Writing – review & editing, Supervision, Conceptualization. **Pietro Ruggieri:** Investigation. **Nicola Bennato:** Investigation. **Lara Righi:** Writing – review & editing, Formal analysis. **Francesca Villa:** Writing – original draft, Visualization, Investigation, Formal analysis, Conceptualization. **Elena Villa:** Writing – review & editing, Supervision, Conceptualization.

Declaration of Competing Interest

The authors declare that they have no known competing financial interests or personal relationships that could have appeared to influence the work reported in this paper.

Data Availability

Data will be made available on request.

Acknowledgements

References

[1] I. Takeuchi, K. Sandeman, Solid-state cooling with caloric materials, Phys. Today 68 (12) (2015) 48–54.

[2] X. Moya, N.D. Mathur, Caloric materials for cooling and heating, Science 370 (2020) 797–803.

[3] K. Engelbrecht, Future prospects for elastocaloric devices, J. Phys. Energy 1 (2019) 021001.

[4] L. Manosa, A. Planes, Solid-state cooling by stress: a perspective, Appl. Phys. Lett. 116 (2020) 050501.

[5] A. Greco, C. Aprea, A. Maiorino, C. Masselli, A review of the state of the art of solid-state caloric cooling processes at room-temperature before 2019, Int. J. Refrig. 106 (2019) 66–88.

[6] P. Kabirifar, A. Žerovnik, Ž. Ahčin, L. Porenta, M. Brojan, J. Tušek, Elastocaloric cooling: state-of-the-art and future challenges in designing regenerative elastocaloric devices, J. Mech. Eng. 65 (2019) 615–630, 11-12.

[7] Report of the International Energy Agency (IEA) "The Future of Cooling: opportunities for energy-efficient air conditioning" (2018).

[8] L. Manosa, A. Planes, Materials with giant mechanocaloric effects: cooling by strength, Adv. Mater. 29 (2017) 1603607.

[9] K. Otsuka, X. Ren, Physical metallurgy of Ti–Ni-based shape memory alloys, Prog. Mater. Sci. 50 (2005) 511–678.

[10] D.C. Lagoudas, Shape Memory Alloys, Springer, (Boston (MA) USA), 2008.

[11] C. Cazorla, Novel mechanocaloric materials for solid-state cooling applications, Appl. Phys. Rev. 6 (2019) 041316.

[12] J. Tušek, K. Engelbrecht, L. Manosa, E. Vives, N. Pryds, Understanding the thermodynamic properties of the elastocaloric effect through experimentation and modelling, Shape Mem. Superelast 2 (2016) 317–329.

[13] I. Aaltio, T. Fukuda, T. Kakeshita, A perspective on elastocaloric effect in Ti–Ni-based shape memory alloys, Shape Mem. Superelast 5 (2019) 230–234.

[14] F. Bruederlin, L. Bumke, C. Chluba, H. Ossmer, E. Quandt, M. Kohl, Elastocaloric cooling on the miniature scale: a review on materials and device engineering, Energy Technol. 6 (2018) 1588–1604.

[15] E.M. Slyusarenko, A.V. Peristyi, E. Yu. Kerimov, I.L. Guzei, M.V. Sofin, Ternary systems of nickel and manganese with transition metals, J. Alloy. Compd. 256 (1997) 115–128.

[16] E.S. Belosludtseva, N.N. Kuranova, N.I. Kourov, V.G. Pushin, A.N. Uksusnikov, Effect of titanium alloying on the structure, the phase composition, and the thermoelastic martensitic transformations in ternary Ni—Mn—Ti alloys, Tech. Phys. 60 (2015) 1330–1334.

[17] H.L. Yan, L.D. Wang, H.X. Liu, X.M. Huang, N. Jia, Z.B. Li, B. Yang, Y.D. Zhang, C. Esling, X. Zhao, L. Zuo, Giant elastocaloric effect and exceptional mechanical properties in an all-d-metal Ni–Mn–Ti alloy: Experimental and ab-initio studies, Mater. Des. 184 (2019) 108180.

[18] Z.Y. Wei, E.K. Liu, J.H. Chen, Y. Li, G.D. Liu, H.Z. Luo, X.K. Xi, H.W. Zhang, W. H. Wang, G.H. Wu, Realization of multifunctional shape-memory ferromagnets in all-d-metal Heusler phases, Appl. Phys. Lett. 107 (2015) 022406.

[19] P.L. Potapov, N.A. Polyakova, V.A. Udovenko, E.L. Svistunova, The martensitic structure and shape memory effect in NiMn alloyed by Ti and Al, Z. Metallkd. 87 (1996) 1.

[20] Z. Guan, J. Bai, J. Gu, X. Liang, D. Liu, X. Jiang, R. Huang, Y. Zhang, C. Esling, X. Zhao, L. Zuo, First-principles investigation of B2 partial disordered structure,

martensitic transformation, elastic and magnetic properties of all-d-metal Ni-Mn-Ti Heusler alloys, J. Mater. Sci. Technol. 68 (2021) 103–111.

[21] D. Cong, W. Xiong, A. Planes, Y. Ren, L. Manosa, P. Cao, Z. Nie, X. Sun, Z. Yang, X. Hong, Y. Wang, Colossal elastocaloric effect in ferroelastic Ni-Mn-Ti alloys, Phys. Rev. Lett. 122 (2019) 255703.

[22] V.A. Chernenko, V.A. L'vov, E. Cesari, A. Kosogor, J.M. Barandiaran, Transformation volume effects on shape memory alloys, Metals 3 (2013) 237–282.

[23] E. Hornbogen, Reversibility and hysteresis of martensitic transformations, Phys. Stat. Sol. (b) 172 (1) (1992) 161–172.

[24] Z.Y. Wei, W. Sun, Q. Shen, Y. Shen, Y.F. Zhang, E.K. Liu, J. Liu, Elastocaloric effect of all-d-metal Heusler NiMnTi(Co) magnetic shape memory alloys by digital image correlation and infrared thermography, Appl. Phys. Lett. 114 (2019) 101903.

[25] Guoyao Zhang, Honglin Wang, Zongbin Li, Bo Yang, Haile Yan, Xiang Zhao, Liang Zuo, Colossal elastocaloric effect in a <001>A oriented Ni49Mn33Ti18 polycrystalline alloy, Scr. Mater. 234 (2023) 115584.

[26] Zhi Yang, Daoyong Cong, Yuan Yuan, Yuan Wu, Zhihua Nie, Runguang Li, Yandong Wang, Ultrahigh cyclability of a large elastocaloric effect in multiferroic phase-transforming materials, Mater. Res Lett. 7 (4) (2019) 137–144.

[27] Huilong Hou, Emrah Simsek, Tao Ma, Nathan S. Johnson, Suxin Qian, Cheikh Cissé, Drew Stasak, Naila Al Hasan, Lin Zhou, Yunho Hwang, Reinhard Radermacher, Valery I. Levitas, Matthew J. Kramer, Mohsen Asle Zaeem, Aaron P. Stebner, Ryan T. Ott, Jun Cui, Ichiro Takeuchi, Fatigue-resistant high-performance elastocaloric materials made by additive manufacturing, Science 366 (2019) 1116–1121.

[28] Jiajing Yang, Honglin Wang, Zongbin Li, Naifu Zou, Haile Yan, Bo Yang, Liang Zuo, Crystallography of stress-induced martensitic transformation and giant elastocaloric effect in a <001>A textured Ni27Cu21Mn46Sn6 shape memory alloy, Acta Mater. 263 (2024) 119546.

[29] K. Otsuka, X. Ren, Physical metallurgy of Ti–Ni-based shape memory alloys, Prog. Mater. Sci. 50 (2005) 511–678.

[30] Muhammad Imran, Xuexi Zhang, Recent developments on the cyclic stability in elastocaloric materials *Materials and Design* 195 (2020) 109030.

[31] P. Chowdhury, L. Patriarca, G. Ren, H. Sehitoglu, Molecular dynamics modeling of NiTi superelasticity in presence of nanoprecipitates, Int. J. Plast. 81 (2016) 152–167.

[32] F. Villa, E. Bestetti, R. Frigerio, M. Caimi, C. Tomasi, F. Passaretti, E. Villa, Elastocaloric properties of polycrystalline samples of NiMnGaCu ferromagnetic shape memory alloy under compression: effect of improvement of thermoelastic martensitic transformation, Materials 150 (2022) 7123.

[33] F. Villa, M. Tamandi, F. Passaretti, E. Bassani, E. Villa, Promising elastocaloric properties of sintered polycrystalline NiMnGa produced by open die pressing, J. Mater. Sci. 58 (2023) 15240–15250.

[34] A. Le Bail, Whole powder pattern decomposition methods and applications: a retrospection, Powder Diffr. 20 (4) (2005) 316–326.

[35] D. Liu, J. Gou, Z. Xu, Y. Liu, T. Ma, Atomic scale understanding the periodic modulation in ferroelastic alloy Ni-Mn-Ti, Acta Mater. 248 (2023) 118768.

[36] E. Villa, C. Tomasi, A. Nespoli, F. Passaretti, G. Lamura, F. Canepa, J. Mater. Res. Technol. 9 (2) (2020) 2259–2266.

[37] P. Mullner, A.H. King, Deformation of hierarchically twinned Martensite, Acta Mater. 58 (2010) 5242–5261.

[38] G.J. Pataky, E. Ertekin, H. Sehitoglu, Elastocaloric cooling potential of NiTi, Ni2FeGa, and CoNiAl, Acta Mater. 96 (2015) 420–427.

[39] J. Tusek, K. Engelbrecht, L.P. Mikkelsen, N. Pryds, Elastocaloric effect of Ni-Ti wire for application in a cooling device, J. Appl. Phys. 117 (2015) 124901.